

WISE morphological study of Wolf-Rayet nebulae

J.A. Toalá¹, M.A. Guerrero¹, G. Ramos-Larios², and V. Guzmán²

¹ Instituto de Astrofísica de Andalucía, IAA-CSIC, Glorieta de la Astronomía s/n, E-18008, Granada, Spain; toala@iaa.es

² Instituto de Astronomía y Meteorología, Av. Vallarta No. 2602, Col. Arcos Vallarta, C.P. 44130, Guadalajara, Jalisco, Mexico.

Preprint online version: March 5, 2018

ABSTRACT

We present a morphological study of nebulae around Wolf-Rayet (WR) stars using archival narrow-band optical and *Wide-field Infrared Survey Explorer* (WISE) infrared images. The comparison among WISE images in different bands and optical images proves to be a very efficient procedure to identify the nebular emission from WR nebulae, and to disentangle it from that of the ISM material along the line of sight. In particular, WR nebulae are clearly detected in the WISE W4 band at 22 μm . Analysis of available mid-IR *Spitzer* spectra shows that the emission in this band is dominated by thermal emission from dust spatially coincident with the thin nebular shell or most likely with the leading edge of the nebula. The WR nebulae in our sample present different morphologies that we classified into well defined WR bubbles (bubble *B*-type nebulae), clumpy and/or disrupted shells (clumpy/disrupted *C*-type nebulae), and material mixed with the diffuse medium (mixed *M*-type nebulae). The variety of morphologies presented by WR nebulae shows a loose correlation with the central star spectral type, implying that the nebular and stellar evolutions are not simple and may proceed according to different sequences and time-lapses. We report the discovery of an obscured shell around WR 35 only detected in the infrared.

Key words. circumstellar matter — infrared sources — Stars: massive — Stars: Wolf-Rayet — Stars: winds

1. Introduction

Massive stars ($M_i \gtrsim 30 M_\odot$) end up their lives as Wolf-Rayet (WR) stars. Before entering the WR phase, these stars evolve through the red or yellow supergiant (RSG or YSG) or luminous blue variable (LBV) phases, depending on the initial stellar mass, and eject their envelopes via copious slow winds expanding at 10–100 km s^{-1} . When a fast stellar wind (1000–2,000 km s^{-1}) develops during the WR phase, it sweeps up the previously ejected slow RSG/LBV wind material to form a WR nebula. The swept-up circumstellar material is photoionized by the central star and has temperatures of $\sim 10^4$ K.

WR nebulae present different morphological features such as bubbles, blowouts, clumps, filaments, and diffuse emission. These nebulae are observable at all frequencies of the electromagnetic spectrum: radio (e.g., Arnal & Cappa, 1996; Arnal et al., 1999; Cappa et al., 2002, 2008, 2009), infrared (IR; e.g., van Buren & McCray, 1988; Gvaramadze et al., 2010a; Mauerhan et al., 2010; Wachter et al., 2010; Flagey et al., 2011; Stringfellow et al., 2012; Wachter et al., 2011), optical (e.g., Chu, 1982; Treffers & Chu, 1982a; Chu et al., 1983; Gruendl et al., 2000; Stock & Barlow, 2010; Fernández-Martín et al., 2012), and X-rays (e.g., Bochkarev, 1988; Wrigge et al., 1994; Wrigge, 1999; Chu et al., 2003; Wrigge & Wendker, 2002; Wrigge et al., 2005; Zhekov & Park, 2011; Toalá et al., 2012, 2015).

Chu (1981) started a series of works proposing a coherent morphological classification of nebulae associated with WR stars as: *R* - radiatively excited H II regions, *E* - stellar ejecta, and *W* - wind-blown bubbles (see Chu, 2003, for an updated review of the morphology of WR nebulae). The *R*-type nebulae present optical emission lines with widths comparable to those in ordinary H II regions, and are further divided into amorphous H II regions (R_a) and shell-structured H II regions (R_s). The *E*-type

nebulae, characterized by their highly clumpy appearance and irregular velocity field, were proposed to form through sudden episodes of mass ejection. Finally, the *W*-type nebulae present a thin sheet of gas and filaments curving around a WR star which is close to the geometric center of the nebula or offset toward the brightest rim. *W*-type nebulae are predicted by numerical simulations of the circumstellar medium (CSM) around WR stars (e.g., García-Segura et al., 1996a,b; Freyer et al., 2003, 2006; Toalá & Arthur, 2011). Using this classification scheme, Stock & Barlow (2010) extended and revised the morphologies of a sample of southern WR nebulae.

Chu (1981) found a correlation, later confirmed by Chu et al. (1983), between nebular morphology and spectral type of the central WR star: WC stars are mostly associated with R_s nebulae, whereas the central stars of *W* nebulae are mostly early WN stars and those of *E* nebulae are exclusively of spectral type WN8. This correlation was interpreted in terms of nebular evolution, so that *W* nebulae, at an early nebular phase, will precede R_s nebulae (Chu et al., 1983).

The classification scheme described above is very demanding observationally. It requires both direct line imaging and spectroscopic campaigns to investigate the morphology, kinematics, and abundances of the ionized material in order to disentangle the emission of the WR nebulae from that of the ISM. In the recent years, mid-IR observations have proved very useful to study WR nebulae or to discover new nebulae around evolved stars (e.g., Wachter et al., 2010). In particular, *Spitzer* observations in the 24 μm band have been found to be sensitive to the WR nebular emission, whereas the near-IR *K* and mid-IR 8 μm bands trace mainly the emission of material along the line of sight (e.g., Wachter et al., 2010; Stringfellow et al., 2012). Mid-IR observations of WR nebulae are thus a promising tool to study these objects.

Here we present *Wide-field Infrared Survey Explorer* (*WISE*; Wright et al., 2010) images of a sample of 31 WR stars and compare them with narrow-band optical images (Section 2). This observational approach provides a straightforward method to identify nebulae around WR stars, clearly separating its emission from that of the ISM. The nature of the emission of WR nebulae in different *WISE* bands is investigated using mid-IR *Spitzer* spectra (Section 3). Their morphologies have been broadly grouped into three morphological types that can be interpreted in the framework of the evolution of the previously ejected dense wind through different evolutive paths (Section 4).

2. Observations

We have searched the *WISE* Preliminary Release Database made public in April 2011 for IR images of stars in the VIIth catalogue of Galactic Wolf-Rayet stars (van der Hucht, 2001) and found a sample of 31 WR stars with available data¹. To compare their IR and optical morphologies, we have selected H α line images of these nebulae in the Super COSMOS Sky Survey (Parker et al., 2005), or STScI Digitized Sky Survey (DSS)² from the Second Palomar Observatory Sky Survey (POSS-II). For a few cases, we have used the [O III] and H α images presented in Gruendl et al. (2000) that have been kindly provided by Y.-H. Chu and R.A. Gruendl. The names and coordinates of the sources in our sample are listed in Table 1 together with the distance, height over the Galactic Plane, and the spectral type and wind terminal velocity of their central stars. Table 1 also identifies the telescope or public database used to acquire the optical images used in this paper. Note that for the specific cases of WR 7 and WR 136 we have also used the existing DSS blue band to complement the morphology seen in the DSS red band³.

The *WISE* images of the WR nebulae in Table 1 were downloaded from the *WISE* Image search tool at the NASA/IPAC Infrared Science Archive (IRSA). To study the IR morphology of these nebulae, we will use the W2 ($\lambda_c=4.6\mu\text{m}$), W3 ($\lambda_c=12\mu\text{m}$), and W4 ($\lambda_c=22\mu\text{m}$) bands. The spatial resolutions for the W2, W3, and W4 bands are 6'1, 6'4, 6'5, and 12'0, respectively, with an astrometric accuracy for bright sources better than 0'15.

2.1. IRS spectra

To help us interpret the nature of the IR emission of WR nebulae in the *WISE* W3 and W4 bands, we have searched for *Spitzer* InfraRed Spectrograph (IRS) spectroscopic observations in the 10–37 μm range of the WR nebulae in our sample listed in Table 1. We found available spectroscopic observations for a sample of 15 WR nebulae. Whereas the detailed analysis of these spectra will be presented in a subsequent paper (Toalá et al., in prep.), here we will focus on the nebulae around WR 7 (NGC 2359), WR 8, and WR 31a, because there are available high-dispersion spectroscopic observations for these nebulae, as

well as for the background emission from apertures located at their periphery.

The basic calibrated data (BCD) of the IRS observations of these WR nebulae were downloaded from the *Spitzer* Heritage Archive. These data are processed with the *Spitzer* Science Center Pipeline Version S18.18.0, and include high-resolution spectroscopic observations (R~600) obtained using the Short-High (SH, 9.9–19.6 μm) and Long-High (LH, 18.7–37.2 μm) modules. The targets were observed using apertures with sizes of 13'6×4'5 in the SH module and 22'3×8'9 in the LH module. All the IRS data were reduced using the CUBE Builder for IRS Spectra Maps (*CUBISM*). This tool does not only reduce the IRS data, but it can also be used to analyze the IRS data and to extract one-dimensional spectra. The various processing steps followed within *CUBISM*, including the characterization of noise in the data and the removal of bad pixels, are described by Smith et al. (2007). We note that the *Spitzer* IRS spectra of WR 8 and WR 31a include the stellar continuum from their WR stars, as they were included in the aperture given the small angular size of these nebulae.

3. Interpreting the IR emission of WR nebulae

We present in Figures 1 to 3 and the figures in Appendix A the optical and *WISE* IR images of the WR nebulae listed in Table 1. The inspection of the colour-composite IR pictures of WR nebulae presented in the figures (see Figures 1 to 3) reveals the prevalence of the emission in the *WISE* W4 band at 22 μm (red in these colour-composite pictures). The emission in this band is mostly coincident with the optical H α emission from ionized nebular material (e.g., WR 16 in Fig. 1-bottom panels). This is in agreement with *Spitzer* MIPS 24 μm imaging of nebulae around evolved massive stars (e.g., Gvaramadze et al., 2009, 2010a; Wachter et al., 2010; Flagey et al., 2011). On the other hand, the emission in the W3 band (green in the colour-composite pictures), which is sensitive to cold gas or low ionization material, seems to trace mostly ISM gas along the line of sight (e.g., Fig. 3), with little contribution of emission from the WR nebula in some cases (e.g., S 308 around WR 6, Fig. 1). Some WR nebulae, however, may show bright emission in this band from discrete knots and clumps interior to the nebular shell (e.g., NGC 6888, Fig. A.23). Finally, the W2 band (blue in the colour-composite pictures), which is expected to trace the continuum emission from small grains and the background stellar component (see Flagey et al., 2011), shows emission from stars in the background. For the most dusty cases, the nebulae around WR 7, WR 18, WR 22, and WR 23 the W2 band also includes some nebular emission.

The nature of the emission in the *WISE* W3 and W4 bands has been further investigated using the *Spitzer* IRS high-dispersion background-subtracted spectra of the nebulae around WR 7 (NGC 2359), WR 8, and WR 31a presented in Figure 5. These spectra have been overplotted by the spectral responses of the *WISE* W3 (green) and W4 (red) bands. The spectra of these nebulae imply significant contribution to the emission detected in the *WISE* W3 band by a number of emission lines, including [S IV] $\lambda 10.51\mu\text{m}$, He I $\lambda 10.66\mu\text{m}$, He I $\lambda 11.31, 12.37, 16.21\mu\text{m}$, [Ar V] $\lambda 13.10\mu\text{m}$, and [Ne III] $\lambda 15.55\mu\text{m}$. In sharp contrast, the *WISE* W4 band is mostly dominated by continuum emission probably from thermal dust continuum emission, with weak H I, [Fe II], and [O IV] emission lines. It is interesting to note that the spectrum of WR 7, extracted from a region known to be overabundant in oxygen (Dufour, 1989), does not show bright emission from oxygen lines, but a weak [O IV] $\lambda 25.59\mu\text{m}$ line.

¹ The mid-IR *WISE* images of the nebulae around WR 43abc, WR91, and WR 93 (NGC 3603, RCW 122, and NGC 6357, respectively) were also examined. These stars belong to young stellar clusters, and thus their nebulae are influenced not only by the WR star, but by all stars in the cluster. Their resulting morphologies are complex and difficult to classify. Furthermore, their *WISE* W3 and W4 band images were saturated at their central regions. Accordingly, we discarded these nebulae from our analysis.

² <https://archive.stsci.edu/cgi-bin/dss.form>.

³ The rest of the WR nebulae do not have their corresponding DSS blue band images.

Table 1. Stellar and Nebular Parameters of the WR Sample^a

WR	Nebula ^b	R.A.	Dec.	Galactic Coord.	d	z	Spectral Type	v_{∞}	Optical Observation ^c	Nebular Type
		(J2000)		l, b (°)	(kpc)	(pc)		(km s ⁻¹)		
6	S 308	06 54 13.05	-23 55 42.1	234.76-10.08	1.50	-262	WN4-s	1700	CTIO (H α , [O III])	<i>B</i>
7	NGC 2359	07 18 29.13	-13 13 01.5	227.75-0.13	3.67	-8	WN4-s	1600	SuperCOSMOS/DSS	<i>B</i>
8		07 44 58.22	-31 54 29.6	247.07-3.79	3.47	-229	WN7/WCE+?	1590	SuperCOSMOS	<i>C</i>
16	Anon	09 54 52.91	-57 43 38.3	281.08-2.55	2.37	-105	WN8h	650	SuperCOSMOS	<i>B</i>
18	NGC 3199	10 17 02.28	-57 54 46.9	283.57-0.97	2.20	-37	WN4-s	1800	DSS	<i>C</i>
22	Anon	10 41 17.52	-59 40 36.9	287.17-0.85	3.24	-48	WN7h+O9III-V	1785	DSS	<i>M</i>
23	Anon	10 41 38.33	-58 46 18.8	286.78-0.03	3.24	-2	WC6	2340	DSS	<i>B</i>
30	Anon	10 51 06.01	-62 17 01.8	284.44-2.61	5.83	-263	WC6+O6-8	2100	SuperCOSMOS	<i>M</i>
31a		10 53 59.66	-60 26 44.3	288.94-0.81	8.0	-113	WN11h	365	SuperCOSMOS	<i>B</i>
35	Anon	11 00 22.10	-61 13 51.0	289.97-1.19	17.87	-371	WN6h-w	1100	SuperCOSMOS	<i>C</i>
35b	Anon	11 00 02.30	-60 14 01.0	289.63-0.24	2.19	-9	WN4	...	SuperCOSMOS	<i>M</i>
38	Anon	11 05 46.52	-61 13 49.1	290.57-0.92	5.83	-94	WC4	3200	SuperCOSMOS	<i>M</i>
40	RCW 58	11 06 17.21	-65 30 35.2	292.31-4.83	2.26	-190	WN8h	650	CS (H α , [O III])	<i>C</i>
52	Anon	13 18 28.00	-58 08 13.6	306.50+4.54	1.51	120	WC4	3225	SuperCOSMOS	<i>M</i>
54	Anon	13 32 43.79	-65 01 27.9	307.27-2.50	7.53	-321	WN5-w	1500	SuperCOSMOS	<i>M</i>
55	RCW 78	13 33 30.13	-62 19 01.2	307.80+0.16	6.03	17	WN7 (WNE-w)	1200	SuperCOSMOS	<i>C</i>
65	G320.5-1.4	15 18 21.0	-59 38 10.0	320.54-1.88	3.27	-107	WC7	2100	SuperCOSMOS	<i>M</i>
78	RCW 104	16 24 26.23	-51 32 06.1	332.84-1.48	2.18	-56	WN6-s	2300	CS (H α , [O III])	<i>B</i>
85	RCW 118	17 14 27.13	-39 45 47.0	347.43-0.61	4.66	-50	WN6h-w (WNL)	1400	SuperCOSMOS	<i>C</i>
86	RCW 130	17 18 23.06	-34 24 30.6	352.25+1.85	2.86	92	WC7(+B0III-I)	1855	DSS	<i>M</i>
94	Anon	17 33 07.14	-33 38 23.7	354.60-0.25	3.12	-14	WN5-w	1300	SuperCOSMOS	<i>M</i>
95		17 36 19.76	-33 26 10.9	355.13-0.70	2.09	-26	WC9d	1900	SuperCOSMOS	<i>C</i>
101	Anon	17 45 09.10	-31 50 16.0	357.47-1.43	3.18	-79	WC8	...	SuperCOSMOS	<i>C</i>
102	G2.4+1.4	17 45 47.00	-26 10 29.0	2.38+1.41	5.56	137	WO2	5000	SuperCOSMOS	<i>B</i>
113	RCW 167	18 19 07.36	-11 37 59.2	18.91+1.75	1.79	55	WC8d+O8-9IV	1700	DSS	<i>M</i>
116	Anon	18 27 04.28	-12 22 52.3	19.16-0.32	2.48	-14	WN8h	800	SuperCOSMOS	<i>C (M?)</i>
124	M1-67	19 11 30.88	+16 51 38.2	50.20+3.31	3.36	194	WN8h	710	DSS	<i>C</i>
128	Anon	19 48 32.20	+18 12 03.7	55.62-3.79	9.37	-619	WN4(h)-w	2050	MLO (H α , [O III])	<i>B</i>
131		20 00 19.12	+33 15 51.1	69.90+1.71	11.78	352	WN7h	1400	DSS	<i>C</i>
134	Anon	20 10 14.20	+36 10 35.1	73.45+1.55	1.74	47	WN6-s	1700	MLO (H α , [O III])	<i>C</i>
136	NGC 6888	20 12 06.55	+38 21 17.8	75.48+2.43	1.26	53	WN6(h)-s	1600	DSS (Red, Blue)	<i>B</i>

^a All parameters have been adopted from van der Hucht (2001), but the spectral classification and terminal velocities have been revised according to Hamann et al. (2006) and Sander et al. (2012).

^b The name Anon is given to those nebulae that have not been catalogued as independent objects nebula, as those that are a small portion of a larger nebular region (see Chu, 1981; Chu et al., 1983).

^c CTIO: Cerro Tololo Inter-American Observatory, SuperCOSMOS: Super COSMOS Sky Survey, DSS: STScI Digitized Sky Survey, CS: Curtis-Schmidt, and MLO: Mount Laguna Observatory.

It is thus concluded that the emission from WR nebulae in the *WISE* W3 band is dominated by H I and forbidden emission lines, mostly of [S IV] and [Ne III], with little contribution to the observed emission from dust thermal continuum. Interestingly, the spatial correspondence between broad arc-like patches of emission in the W3 image of S 308 around WR 6 and diminished emission in H α (Fig. 1) seems to imply absorption of nebular emission by dust on the foreground. As expected, the W3 band traces material in the ISM in most cases. Meanwhile, the emission in the *WISE* W4 band, tracing mostly the optical nebular shells, corresponds to thermal continuum emission, with very little contribution from H I, [Fe II], and [O IV] emission lines. These results are not in disagreement with the IRS spectrum of the WR bubble MB 3957, which is dominated by emission lines of iron, sulfur and neon, but also includes an additional contribution of thermal dust emission (Flagey et al., 2011). Otherwise, the *Spitzer* MIPS 24 μ m images of planetary nebulae include important contributions from the [O IV] λ 25.89 μ m and [Ne V] λ 24.3 μ m emission lines (e.g. Chu et al., 2009), unlike the *WISE* W4 images of WR nebulae. The spatial resolution of the *WISE* W4 band images, $\approx 12''$, does not allow us to determine whether the dust in WR nebulae is spatially coincident with the ionized material or is found at the leading edge of the optical WR nebulae.

4. Morphological classification of WR nebulae

The images of the WR nebulae presented in Figures 1 to 3 are examples of the variety of morphologies from complete shells, arcs (incomplete shells), clumps, and filaments to diffuse, featureless emission. A close inspection to all WR nebulae in our sample and the comparison between optical and IR morphologies has led us to classify them into three broad morphological types:

– *B* - WR Bubble.

These nebulae present a thin shell or bubble both in optical and IR, mostly in the W4 band. Examples of these nebulae are those around WR 6 (S 308) and WR 16 (see Fig 1).

– *C* - Clumpy/Disrupted WR bubbles.

These nebulae present clumpy H α and IR images and/or incomplete arcs or shells. The W4 images reveal for a significant number of cases that the optical and IR clumps are spatially coincident with bow shock-like features. Archetypes of these WR nebulae are those around WR 8 and WR 18, WR 35 and WR 40 (see Fig. 2 and 4).

– *M* - Mixed WR nebulae.

These nebulae do not present a clear correspondence between the optical and IR images. Indeed, they do not show a clearly defined IR morphology, with a noticeable lack of emission in the *WISE* W4 band. Examples of these nebulae are those around WR 35b and WR 52 (see Fig. 3).

Our classification of the WR nebulae is listed in the last column of Table 1. We note that sometimes the assignation of a

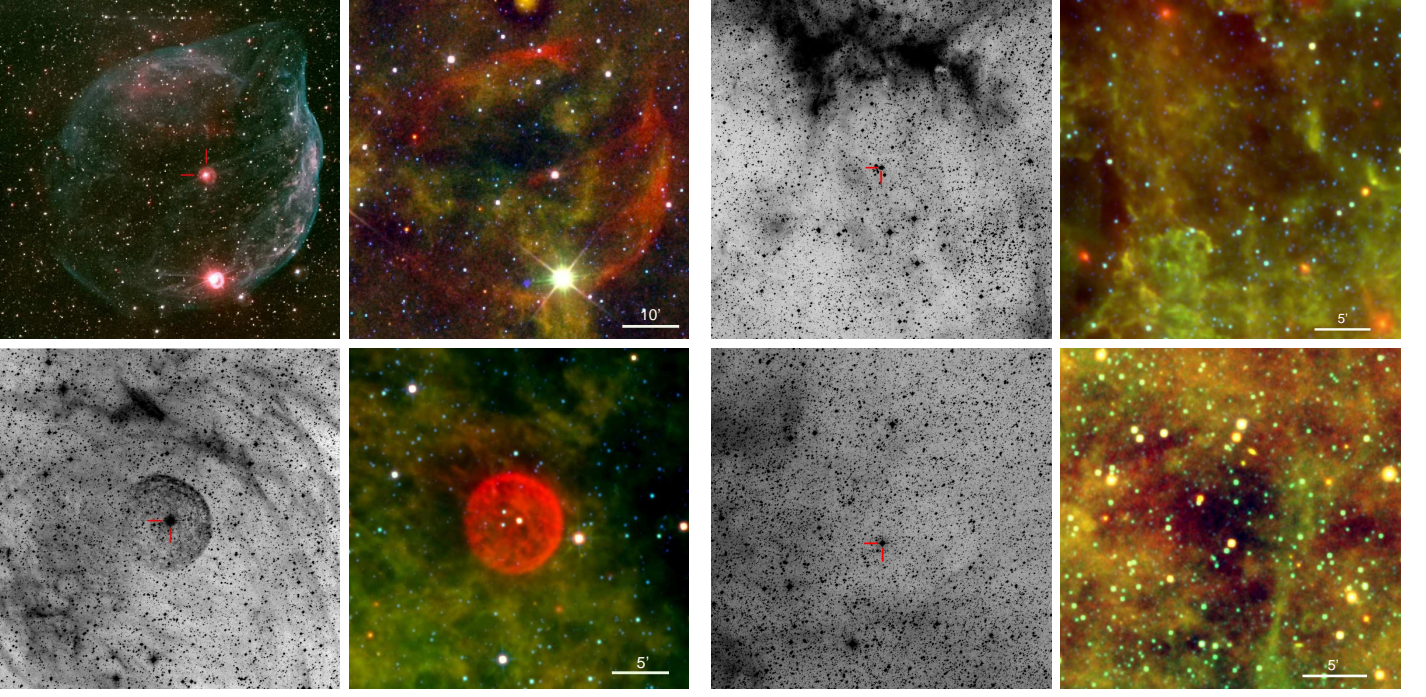


Fig. 1. Examples of WR nebulae with a \mathcal{B} type morphology: WR 6 (top panels) and WR 16 (bottom panels). Left panels show the optical morphology while right panels show the *WISE* W2 (blue), W3 (green), and W4 (red) color-composite picture. The central WR stars are marked with red lines in the optical images. The colour-composite optical picture of WR 6 has been done using $H\alpha$ (red) and $[O\text{ III}]$ (blue) narrow-band images. North is up, east to the left.

Fig. 3. Same as Fig. 1 but for the cases of WR nebulae with a \mathcal{M} morphology: WR 35b (top panels) and WR 52 (bottom panels).

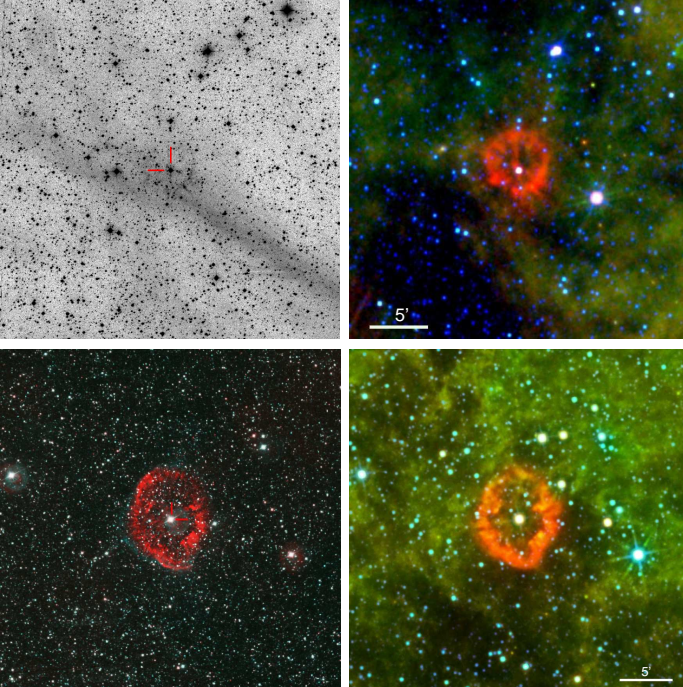


Fig. 2. Same as Fig. 1 but for the cases of WR nebulae with a \mathcal{C} -Clumpy morphology: WR 8 (top panels) and WR 40 (bottom panels). The color-composite optical image of WR 40 has been done using $H\alpha$ (red) and $[O\text{ III}]$ (blue) narrow band images.

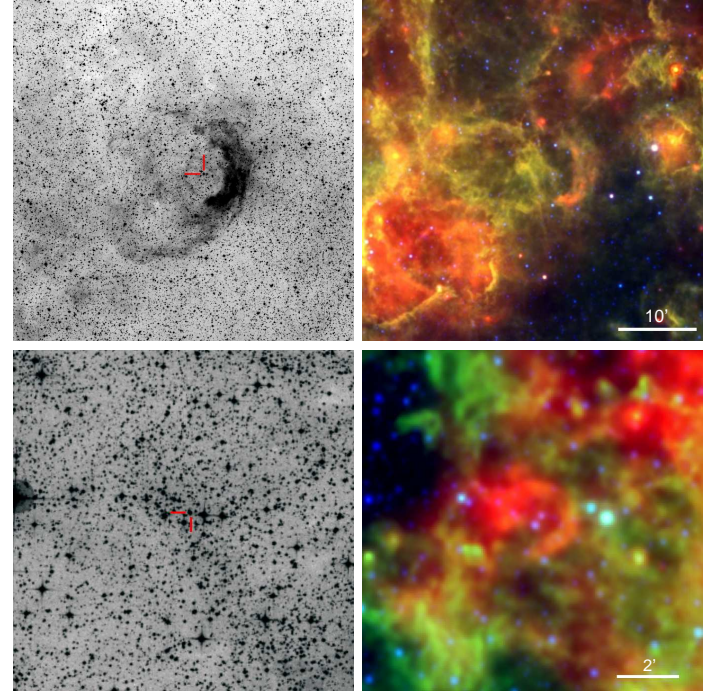


Fig. 4. Same as Fig. 1 but for the cases of WR nebulae with a \mathcal{C} -Disrupted morphology: WR 18 (top panels) and WR 35 (bottom panels).

morphological type is difficult given the disparity between the optical and IR images or due to the ambiguous association between the star and the nebula. For instance, the nebula around WR 116 (Fig. A.17) has been assigned a morphological type \mathcal{C}

in basis of its optical image, but we reckon that a morphological type \mathcal{M} cannot be completely excluded by its IR counterpart.

4.1. Notes on individual objects

4.1.1. WR 35 and its obscured shell

We report the previously unknown partial shell around WR 35. This shell, clearly detected in the *WISE* W4 band (Fig. 4-bottom panels), has a size $\sim 2'.0 \times 1'.5$ and opens towards the southeast of WR 35. In contrast, the $H\alpha$ image from the Super COSMOS Sky Survey only detects emission from an ionized cloud southwest of WR 35 which does not coincide spatially with the IR shell. A similar case of detection of an obscured shell has been claimed by Wachter et al. (2011) for WR 8, although an optical nebulosity was previously reported by Stock & Barlow (2010). The high frequency of discovery of obscured shells around massive stars in *Spitzer* MIPS 24 μm images has led to the suggestion that such shells may be ubiquitous among these stars (e.g., Gvaramadze et al., 2010a; Wachter et al., 2010).

4.1.2. A bipolar nebula around WR 85

The nebula RCW 118 around WR 85 has been described as a bipolar nebula based on $H\alpha$ images obtained by Marston et al. (1994a,b). This bipolar structure is hinted in the *WISE* W4 image by the red patches to the northeast and southwest of WR 85 (Fig. A.11-right). This IR image is certainly reminiscent of the optical image of the nebula NGC 6164-5 around the O6 star HD 148937 (Bruhweiler et al., 1981; Dufour et al., 1988).

4.2. Comparison with previous morphological classifications

Previous imaging studies of WR nebulae have disclosed a rich morphological variety among them (e.g., Chu et al., 1983; Gruendl et al., 2000; Stock & Barlow, 2010). The most complete classification scheme of WR nebulae is that originally introduced by Chu (1981) and more recently described by Chu (2003). This classification scheme relies on narrow-band optical images, kinematics, and information on the chemical abundances to define the presence of bubbles and their expansion rate and kinematical age. Meanwhile, our classification scheme of WR nebulae is supported by the comparison between narrow-band optical (mostly $H\alpha$) and mid-IR *WISE* images, the latter being very useful to unveil obscured shells and to disentangle the nebular emission from background diffuse and ISM emission as discussed in Section 3.

The comparison between these two morphological classifications of WR nebulae in Table 2 reveals a good agreement. This is excellent for the wind-blown bubbles (our \mathcal{B} nebulae and the W class), as these are the most easy to spot either in direct images or kinematical data. Indeed, all our \mathcal{B} nebulae are classified as W , and only 4 W objects are classified as C nebulae because their mid-IR morphology.

This consistency is confirmed by the comparison between optical images in the $H\alpha$ and $[\text{O III}]$ emission lines that has been shown by Gruendl et al. (2000) to be very helpful to reveal the expansion of shock fronts outside the main nebular shell. For example, in the case of RCW 104 around WR 75 (Figure A.10), the $H\alpha$ line image does not show any morphological characteristic of a round shell, thus implying a classification as a C -type nebula. Instead, the $[\text{O III}]$ morphology implies a \mathcal{B} -type. On the contrary, the nebula M 1-67 around WR 124 shows no evidence of an $[\text{O III}]$ front (Fernández-Martín et al., 2013, and references

Table 2. Comparison of WR Nebula Morphology Classification

WR	This paper	Previous works	References
6	\mathcal{B}	W/E	1,2,3,4
7	\mathcal{B}	W	1,3,4,5
8	C	E	4
16	\mathcal{B}	W	4,7
18	C	W	1,3,4,8
22	\mathcal{M}	W	3,6
23	\mathcal{B}	W	1,3,7
38	\mathcal{M}	Ring?	7
40	C	E	1,3,4,8
52	\mathcal{M}	R_s	1,3,9
54	\mathcal{M}	Ring?	6
55	C	R_a	1,3,9
68	\mathcal{M}	Ring	6
75	\mathcal{B}	W/E	1,3,4,8
85	C	R_s	1,3,9
86	\mathcal{M}	...	6
94	\mathcal{M}	...	7
95	C	...	6
101	C	Ring?	7
102	\mathcal{B}	W/E	4,7
124	C	E	1,3,4,10
128	\mathcal{B}	W/R_s	3,11
131	C	$H II$	1,3,10
134	C	W	1,3,12
136	\mathcal{B}	W/E	1,3,4,12

Refs.— (1) Chu (1981), (2) Chu et al. (1982), (3) Chu et al. (1983), (4) Stock & Barlow (2010), (5) Treffers & Chu (1982a), (6) Marston et al. (1994a), (7) Marston et al. (1994b), (8) Chu (1982), (9) Chu & Treffers (1981b), (10) Chu & Treffers (1981a), (11) Gruendl et al. (2000), (12) Treffers & Chu (1982b).

therein), but its kinematics reveals an expanding shell consisting of numerous condensations (Solf & Carsenty, 1982). While these findings may raise doubts for the classification of WR nebulae for which $[\text{O III}]$ images and kinematics are not available, we note that in all these nebulae the outer expanding shell is noticeably much fainter than the shells detected in our \mathcal{B} -type nebulae. This points to an intrinsic difference between the two morphological types.

As for the \mathcal{M} nebulae, only two have previous definite morphology (Chu, 1991). The nebula around WR 22 is described by Chu (1991) as a possible wind-blown bubble, although no evidence for such a bubble is revealed in *WISE* images (Figure A.2). Similarly, the nebula around WR 52 is categorized as an R_s nebula in basis of kinematical data, but the nebula is rather inconspicuous in the IR (Figure 3-bottom panels).

4.3. Interpreting the morphology of WR nebulae

The main morphological characteristics of WR nebulae result from the interactions of the WR wind and the intense UV radiation with the slow wind ejected previously by the progenitor. The most basic evolutionary path of a WR nebula, as reproduced by multiple simulations (e.g., García-Segura & Mac Low, 1995; García-Segura et al., 1996a,b; Freyer et al., 2003; van Marle et al., 2005; Freyer et al., 2006; Arthur, 2007a,b; van Marle et al., 2007; Dwarkadas, 2007; Toalá & Arthur, 2011), implies a massive star ejecting a significant fraction of its mass during a RSG or LBV phase through a spherical, slow ($10\text{--}100 \text{ km s}^{-1}$) and dense wind. In the

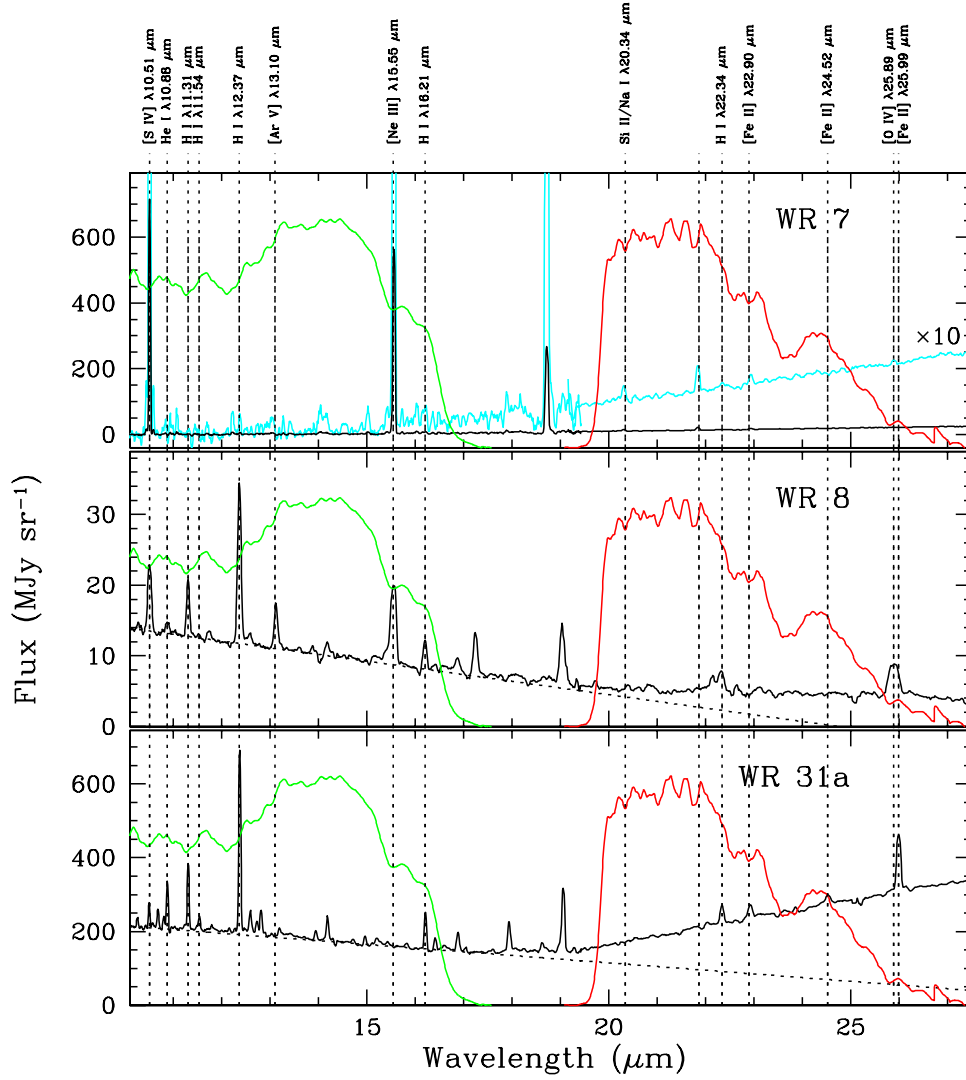


Fig. 5. *Spitzer* IRS SH and LH spectra of the nebulae around WR 7, WR 8, and WR 31a. The spectral responses of the W3 (green) and W4 (red) *WISE* bands normalized to arbitrary values are overplotted on the spectra. The nebular spectrum of WR 7 corresponds to the patch of bright red emission (the *WISE* W4 band) towards the northwest shown in Figure A.1. This spectrum has been plotted at two different intensity levels to highlight the low level emission. The contribution of the stellar emission of WR 8 and WR 31a to the nebular spectra can be roughly reproduced by a black-body model (dashed line).

final stage of stellar evolution, during the WR phase, this CSM will be swept up by the WR fast stellar wind ($v_{\infty} \gtrsim 10^3 \text{ km s}^{-1}$), creating at early times a WR bubble (\mathcal{B} -type nebulae). Later on, the WR bubble will be disrupted due to Rayleigh-Taylor and thin shell instabilities (\mathcal{C} -type nebulae) and the resulting filaments and clumps will later mix with the ISM (\mathcal{M} -type nebulae).

Additional processes may alter this general scheme. For instance, the proper motion of the star or a density gradient in the ISM may compress and brighten the nebula as it interacts with its surroundings, resulting in incomplete shells and arcs. Stellar rotation can also introduce changes in the stellar evolution (e.g., Meynet & Maeder, 2003; Ekström et al., 2012) and produce, for instance, anisotropic stellar winds. In the case of non-spherical (e.g., bipolar or clumpy) ejections of material seen in some LBV nebulae (e.g., MN13 and MN79; Humphreys, 2010; Gvaramadze et al., 2010a), the wind-wind interaction will give place to the immediate formation of clumps or filaments,

forming directly a \mathcal{C} -type nebulae with no \mathcal{B} -type nebula in between. The large-scale structure of the ISM may also alter the morphology of WR nebulae.

Since WR nebulae can form through different morphological sequences, we should not expect a tight correlation between nebular morphology and the star evolutionary stage implied by its WR spectral type (e.g., Moffat, 1995; Maeder, 1997). Certainly, \mathcal{M} -type nebulae can be expected preferentially around evolved WR stars, whereas the central stars of \mathcal{B} and \mathcal{C} -type nebulae can be expected to have late spectral types (Chu, 1981; Chu et al., 1983). This correspondence is further complicated by the time-lapse spent by a WR star on the different WR sub-phases which depends strongly on different factors (initial mass, rotation, initial metallicity; e.g., Maeder, 1991; Meynet & Maeder, 2005; Georgy et al., 2012). A star may even miss a WR sub-phase; for example, the stellar evolution models at solar metallicity of Meynet & Maeder (2003) predict that a rotating $25 M_{\odot}$ star will

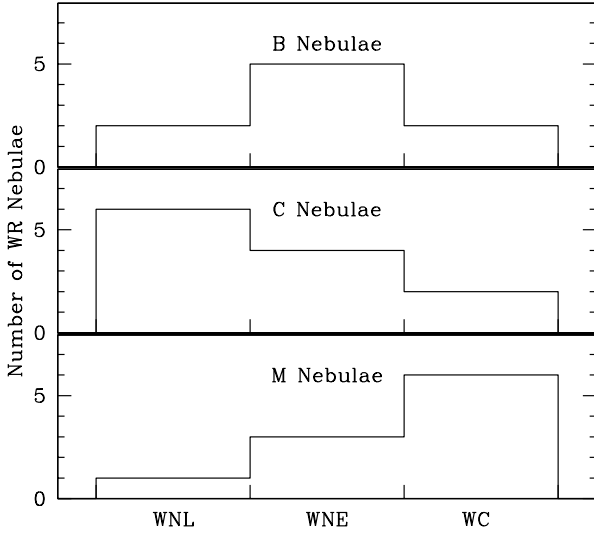


Fig. 6. Distribution of the different morphological types of WR nebulae depending on the spectral types of their WR central stars.

not enter the WNE and WC stages. Therefore, for those particular models, any type of WR nebulae can be found around WNL stars because the long duration of this phase or even the lack of the WNE stage. On the other hand, for the case of non-rotating models, which predict comparable durations of the WNL and WNE phases, we may expect *B*-type nebulae around these two types of stars.

To better quantify these relationships, we show in Figure 6 the distributions of nebular morphology and stellar spectral type among the WR nebulae in our sample. Five out of the nine *B* nebulae have WNE stars and two others have WNL spectral types, whereas only two are early WC stars. The WNL stars WR 16 (WN8) and WR 31a (WN11) are surrounded by small-sized bubbles (2.8 and 1.2 pc in radius, respectively), and the WC WR 23 (WC6) and WR 102 (WO2) stars by large bubbles (16 and 4 pc in radius, respectively). Nebulae with *C*-type morphology harbor mostly late WN7-WN8 stars (6 out of 12) or WNE stars (4 out of 12), with only two WC stars (WR 95 and WR 101). On the contrary, *M* nebulae have a significant fraction of early WC stars (6 out of 10) and a very small number of WNL stars (1 out of 10). This confirms previous suggestions that WR bubbles are associated to late WN stars and *C*-type to WC stars. Most *C* nebulae had been previously classified either as *W* or *E* nebulae, but we notice some contamination of *R_a* and *R_s* nebulae, and even objects of uncertain morphology. This indicates that *C* nebulae have a variety of kinematical and chemical properties. This is also the case for their WR central stars which can be linked to different evolutionary paths leading to a *C*-nebula morphology.

5. Comparison with previous mid-IR studies

The extinction by dust in the Galactic Plane makes difficult the search for WR nebulae at optical wavelengths. The detection of the mid-IR emission (thermal dust, molecules, PAHs, ...) of shells around evolved stars may provide an alternative method for the direct identification of these nebulae. Mid-IR observations have indeed allowed the detection of young PNe (e.g., Morris et al., 2006; Fesen & Milisavljevic, 2010) and LBV neb-

ulae (e.g., Gvaramadze et al., 2010b; Wachter et al., 2010). Not unexpectedly, *Spitzer* MIPS 24 μ m data have been used to discover new WR stars by the direct detection of mid-IR emission from its circumstellar nebula (e.g., WR 121b, Gvaramadze et al., 2010c). Two outstanding examples are the identification of the interacting nebulae around the WN9h type stars, WR 120bb and WR 120bc, by Burgemeister et al. (2013) and the identification of a WR nebula in the Large Magellanic Cloud reported by Gvaramadze et al. (2014). Of course, the direct identification of circumstellar nebulae around WR stars in the mid-IR 24 μ m band requires a mandatory spectroscopic characterization of the nebular emission, but it is important to emphasize the simplicity and potential of the mid-IR method.

In this paper, we have taken advantage of the similarities between the spectral responses of the *Spitzer* MIPS 24 μ m and *WISE* W4 22 μ m bands to investigate the circumstellar medium around a significative sample of known Galactic WR stars. By identifying the mid-IR counterparts of these WR nebulae, we have assessed their true extent, disentangling the optical emission of the circumstellar shells from that of the ISM along the line of sight. New mid-IR shells (e.g., WR 35, Fig. 4-bottom panels) have also been discovered. It is worth mentioning here the notable case of NGC 3199, the nebula around WR 18 (see Fig. 4-top panels). Stock et al. (2011) derived the chemical abundances for a bright H α nebular clump and concluded they were consistent with those of the Galactic H II region M 17 on which NGC 3199 is projected. Accordingly, they proposed that NGC 3199 consists mainly of swept-up ISM material. A careful registration of the location of the $\sim 15''$ VLT/UVES slit used by Stock et al. (2011) on the *WISE* images shows that this small slit does not include the emission detected in the W4 band (i.e., nebular material), but it is located on a spot of bright emission in the W3 band (i.e., ISM material). These findings cast doubt on the ISM abundances implied by those authors for NGC 3199 and rather support those reported by Marston (2001).

6. Summary and conclusions

We have examined *WISE* IR images of a sample of 31 WR stars to study their nebular morphologies in mid-IR bands. We have then compared the emission in the *WISE* images with optical H α and (in some cases) [O III] emission line images. The variety of morphologies of WR nebulae can be classified as bubble *B*-type nebulae, clumpy/disrupted *C*-type nebulae, and mixed *M*-type nebulae.

We have used *Spitzer* IRS spectra of some WR nebulae to investigate the nature of the IR emission of WR nebulae in the different *WISE* bands (Toalá et al. in preparation). According to previous IR studies of evolved massive stars, we find that the emission in the *WISE* W4 band of *B* and *C*-type nebulae most likely traces dust associated to the WR nebula. On the other hand, the *WISE* W3 band is mainly tracing the emission of material along the line of sight of the nebula, which results in diminished emission at optical wavelengths. We emphasize that the acquisition of mid-IR images of WR nebulae, especially for wavelengths above 20 μ m, is very useful to disentangle the emission from the WR nebula from that of the ISM. This provides a less demanding observational approach for the identification and study of WR nebulae than those based on optical images and spectra. The discovery of an obscured shell around WR 35 which is detected only at 22 μ m in the W4 band *WISE* images or the capability to distinguish the nebular material of NGC 3199 around WR 18 from that of the Galactic H II region M 17 clearly illustrate the advantages of mid-IR observations of WR nebulae.

We find a loose correlation between nebular morphology and stellar spectral type, also claimed in the past, but we note that this correlation is complicated by the different evolutionary sequences of WR nebulae and the dependence of the stellar evolution in these phases with initial mass and composition, and stellar rotation.

Acknowledgments

We would like to thank the referee, Margaret Meixner, for helpful comments. JAT acknowledges CSIC JAE-PREDOC (Spain) student grant 2011-00189. JAT and MAG are partially funded by grants AYA 2008-01934 and AYA 2011-29754-C03-02 of the Spanish MICINN (Ministerio de Ciencia e Innovación) and MEC (Ministerio de Economía y Competitividad) including FEDER funds. GR-L acknowledges support from CONACyT (grant 177864) and PROMEP (Mexico). We are grateful to Y.-H. Chu and R.A. Gruendl for providing us with the [O III] and H α optical images of S 308, RCW 58, RCW 104, WR 128, and WR 134.

This paper is based on observations from the *Wide-field Infrared Survey Explorer*, which is a joint project of the University of California, Los Angeles, and the Jet Propulsion Laboratory/California Institute of Technology, founded by the National Aeronautics and Space Administration. The Digitized Sky Surveys were produced at the Space Telescope Science Institute under the U.S. Government grant NAG W-2166. The Second Palomar Observatory Sky Survey (POSS-II) was made by the California Institute of Technology with funds from the National Science Foundation, the National Geographic Society, the Sloan Foundation, the Samuel Oschin Foundation, and the Eastman Kodak Corporation.

References

- Arnal, E. M., Cappa, C. E., Rizzo, J. R., & Cichowolski, S. 1999, *AJ*, 118, 1798
- Arnal, E. M., & Cappa, C. E. 1996, *MNRAS*, 279, 788
- Arthur, S. J. 2007a, *Revista Mexicana de Astronomía y Astrofísica Conference Series*, 30, 64
- Arthur, S. J. 2007b, *Diffuse Matter from Star Forming Regions to Active Galaxies*, 183
- Bochkarev, N. G. 1988, *Nature*, 332, 518
- Bruehweiler, F. C., Gull, T. R., Henize, K. G., & Cannon, R. D. 1981, *ApJ*, 251, 126
- Burgemeiste, S., Gvaramadze, V. V., Stringfellow, G. S., et al., 2013, *MNRAS*, 429, 3305
- Cappa, C. E., Goss, W. M., & Pineault, S. 2002, *AJ*, 123, 3348
- Cappa, C. E., Rubio, M., Martín, M. C., & Romero, G. A. 2009, *A&A*, 508, 759
- Cappa, C. E., Vasquez, J., Arnal, E. M., Cichowolski, S., & Pineault, S. 2008, *Mass Loss from Stars and the Evolution of Stellar Clusters*, 388, 151
- Chu, Y.-H. 1981, *ApJ*, 249, 195
- Chu, Y.-H. 1982, *ApJ*, 254, 578
- Chu, Y.-H. 1991, *Wolf-Rayet Stars and Interrelations with Other Massive Stars in Galaxies*, 143, 349
- Chu, Y.-H. 2003, *A Massive Star Odyssey: From Main Sequence to Supernova*, 212, 585
- Chu, Y.-H., Gull, T.R., Treffers, R.R., & Kwitter, K.B. 1982, *ApJ*, 254, 562
- Chu, Y.-H., & Treffers, R. R. 1981a, *ApJ*, 249, 586
- Chu, Y.-H., & Treffers, R. R. 1981b, *ApJ*, 250, 615
- Chu, Y.-H., Treffers, R. R., & Kwitter, K. B. 1983, *ApJs*, 53, 937
- Chu, Y.-H., Guerrero, M. A., Gruendl, R. A., García-Segura, G., & Wendker, H. J. 2003, *ApJ*, 599, 1189
- Chu, Y.-H., Gruendl, R. A., Guerrero, M. A., et al. 2009, *AJ*, 138, 691
- Dufour, R. J. 1989, *RMxAA&A*, 18, 87
- Dufour, R. J., Parker, R. A. R., & Henize, K. G. 1988, *ApJ*, 327, 859
- Dwarkadas, V. V. 2007, *ApJ*, 667, 226
- Ekström, S., Georgy, C., Eggenberger, P., et al. 2012, *A&A*, 537, A146
- Fernández-Martín, A., Vílchez, J. M., Pérez-Montero, E., et al. 2013, *A&A*, 554, A104
- Fernández-Martín, A., Martín-Gordón, D., Vílchez, J. M., et al. 2012, *A&A*, 541, AA119
- Fesen, R. A., & Milisavljevic, D. 2010, *AJ*, 139, 2595
- Flagey, N., Noriega-Crespo, A., Billot, N., & Carey, S. J. 2011, *ApJ*, 741, 4
- Freyer, T., Hensler, G., & Yorke, H. W. 2003, *ApJ*, 594, 888
- Freyer, T., Hensler, G., & Yorke, H. W. 2006, *ApJ*, 638, 262
- García-Segura, G., & Mac Low, M.-M. 1995, *ApJ*, 455, 160
- García-Segura, G., Mac Low, M.-M., & Langer, N. 1996a, *A&A*, 305, 229
- García-Segura, G., Langer, N., & Mac Low, M.-M. 1996b, *A&A*, 316, 13
- Georgy, C., Ekström, S., Meynet, G., et al. 2012, *A&A*, 542, AA29
- Gruendl, R. A., Chu, Y.-H., Dunne, B. C., & Points, S. D. 2000, *AJ*, 120, 2670
- Gvaramadze, V. V., Fabrika, S., Hamann, W.-R., et al. 2009, *MNRAS*, 400, 524
- Gvaramadze, V. V., Kniazev, A. Y., & Fabrika, S. 2010a, *MNRAS*, 405, 1047
- Gvaramadze, V. V., Kniazev, A. Y., Fabrika, S., et al. 2010b, *MNRAS*, 405, 520
- Gvaramadze, V. V., Kniazev, A. Y., Hamann, W.-R., et al. 2010c, *MNRAS*, 403, 760
- Gvaramadze, V. V., Chené, A.-N., Kniazev, A. Y., et al., 2014, *MNRAS*, 442, 929
- Hamann, W.-R., Gräfener, G., & Liermann, A. 2006, *A&A*, 457, 1015
- Humphreys, R. M. 2010, *Hot and Cool: Bridging Gaps in Massive Star Evolution*, 425, 247
- Maeder, A. 1991, *A&A*, 242, 93
- Maeder, A. 1997, *IAU Symposium*, 189, 313
- Marston, A. P., Chu, Y.-H., & García-Segura, G. 1994a, *ApJs*, 93, 229
- Marston, A. P., Yocum, D. R., García-Segura, G., & Chu, Y.-H. 1994b, *ApJs*, 95, 151
- Marston, A. P. 2001, *ApJ*, 563, 875
- Mauerhan, J. C., Wachter, S., Morris, P. W., Van Dyk, S. D., & Hoard, D. W. 2010, *ApJL*, 724, L78
- Meynet, G., & Maeder, A. 2003, *A&A*, 404, 975
- Meynet, G., & Maeder, A. 2005, *A&A*, 429, 581
- Moffat, A. F. J. 1995, *Wolf-Rayet Stars: Binaries; Colliding Winds; Evolution*, 163, 213
- Morris, P. W., Stolyov, S., Wachter, S., et al. 2006, *ApJ*, 640, L179
- Parker, Q. A., Philipps, S., Pierce, M. J., et al. 2005, *MNRAS*, 362, 689
- Sander, A., Hamann, W.-R., & Todt, H. 2012, *A&A*, 540, A144
- Smith, J. D. T., Armus, L., Dale, D. A., et al. 2007, *PASP*, 119, 1133
- Solf, J., & Carsenty, U. 1982, *A&A*, 116, 54
- Stock, D. J., Barlow, M. J., & Wesson, R. 2011, *MNRAS*, 418, 2532
- Stock, D. J., & Barlow, M. J. 2010, *MNRAS*, 409, 1429
- Stringfellow, G. S., Gvaramadze, V. V., Beletsky, Y., & Kniazev, A. Y. 2012, *Proceedings of a Scientific Meeting in Honor of Anthony F. J. Moffat*, 465, 514
- Toalá, J. A., Guerrero, M. A., Chu, Y.-H., & Gruendl, R. A. 2015, *MNRAS*, 446, 1083
- Toalá, J. A., & Arthur, S. J. 2011, *ApJ*, 737, 100
- Toalá, J. A., Guerrero, M. A., Chu, Y.-H., et al. 2012, *ApJ*, 755, 77
- Treffers, R. R., & Chu, Y.-H. 1982b, *ApJ*, 254, 569
- Treffers, R. R., & Chu, Y.-H. 1982a, *ApJ*, 254, 132
- van Buren, D., & McCray, R. 1988, *ApJL*, 329, L93
- van der Hucht, K. A. 2001, *New A Rev.*, 45, 135
- van Marle, A. J., Langer, N., & García-Segura, G. 2005, *A&A*, 444, 837
- van Marle, A. J., Langer, N., & García-Segura, G. 2007, *A&A*, 469, 941
- Wachter, S., Mauerhan, J. C., Van Dyk, S. D., et al. 2010, *AJ*, 139, 2330
- Wachter, S., Cohen, M., & Leisawitz, D. 2011, *Bulletin of the American Astronomical Society*, 43, #333.10
- Wrigge, M., Wendker, H. J., & Wisotzki, L. 1994, *A&A*, 286, 219
- Wrigge, M. 1999, *A&A*, 343, 599
- Wrigge, M., & Wendker, H. J. 2002, *A&A*, 391, 287
- Wrigge, M., Chu, Y.-H., Magnier, E. A., & Wendker, H. J. 2005, *ApJ*, 633, 248
- Wright, E. L., Eisenhardt, P. R. M., Mainzer, A. K., et al. 2010, *AJ*, 140, 1868
- Zhekov, S. A., & Park, S. 2011, *ApJ*, 728, 135

Appendix A: Additional Figures

In this appendix we collect the figures of the rest of the WR nebulae studied in this paper not presented in the main text. The nebulae are those around the WR stars WR 7, WR 22, WR 23, WR 30, WR 31a, WR 38, WR 54, WR 55, WR 68, WR 75, WR 85, WR 86, WR 94, WR 95, WR 101, WR 102, WR 113, WR 116, WR 124, WR 128, WR 131, WR 134, and WR 136.

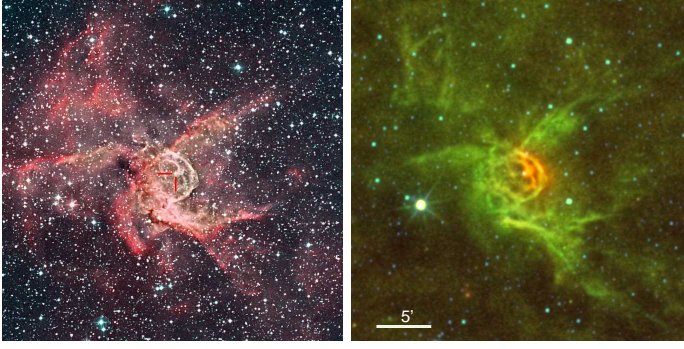


Fig. A.1. Optical (left) and mid-IR *WISE* (right) images of WR 7 (NGC 2359). See Table 1 for details of the optical image. The central WR star is marked with red lines in the left panel. North is up, East to the left.

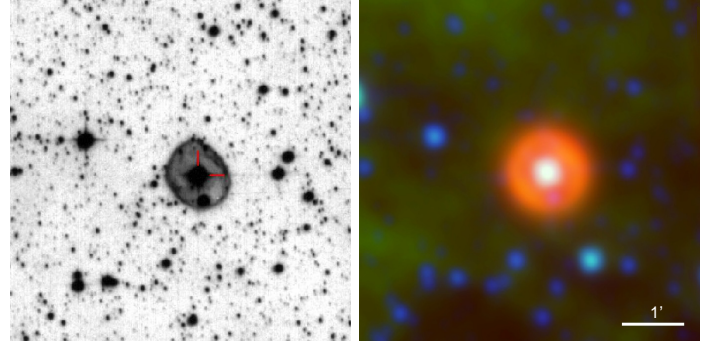


Fig. A.5. Same as Fig. A.1 for WR 31a.

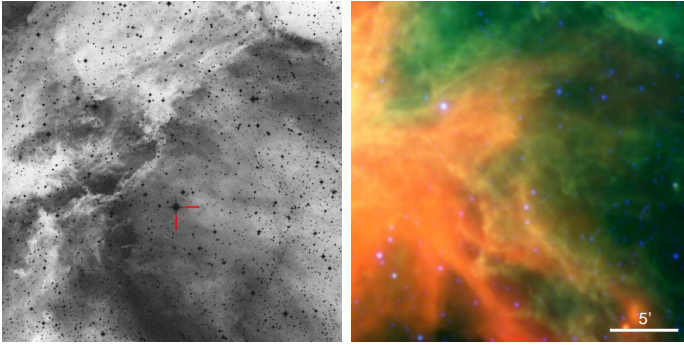


Fig. A.2. Same as Fig. A.1 for WR 22.

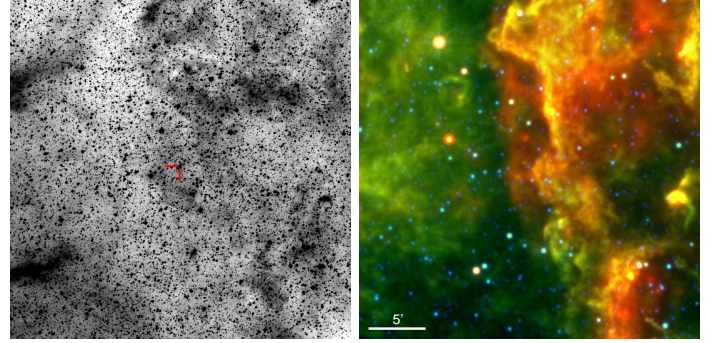


Fig. A.6. Same as Fig. A.1 for WR 38.

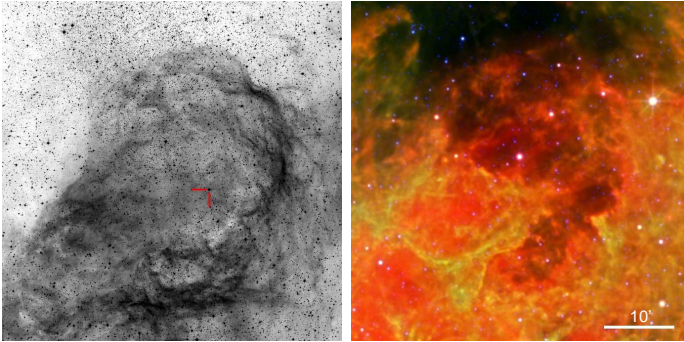


Fig. A.3. Same as Fig. A.1 for WR 23.

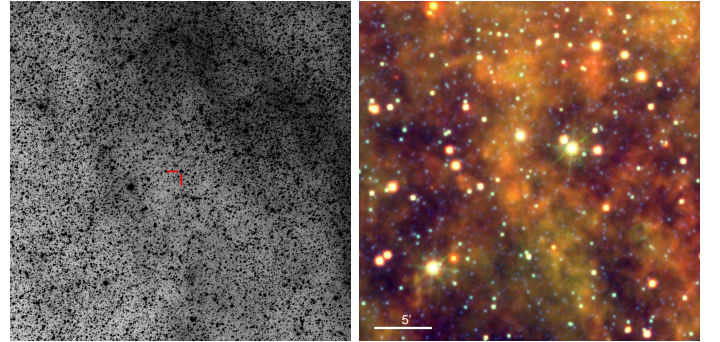


Fig. A.7. Same as Fig. A.1 for WR 54.

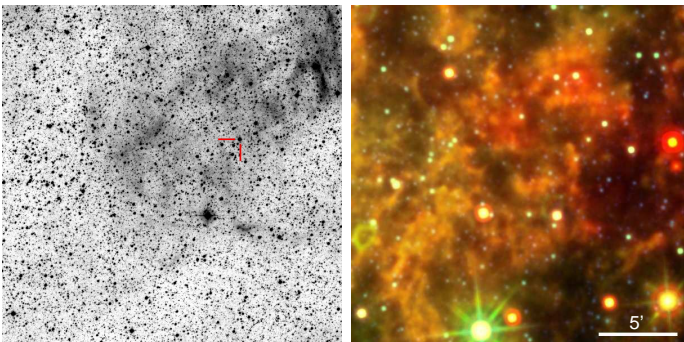


Fig. A.4. Same as Fig. A.1 for WR 30 (Anon).

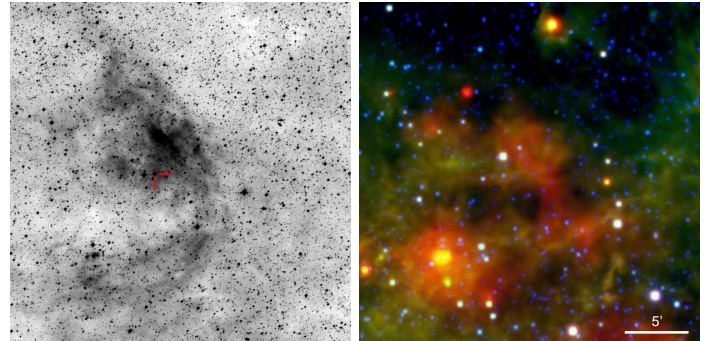


Fig. A.8. Same as Fig. A.1 for WR 55 (RCW 78).

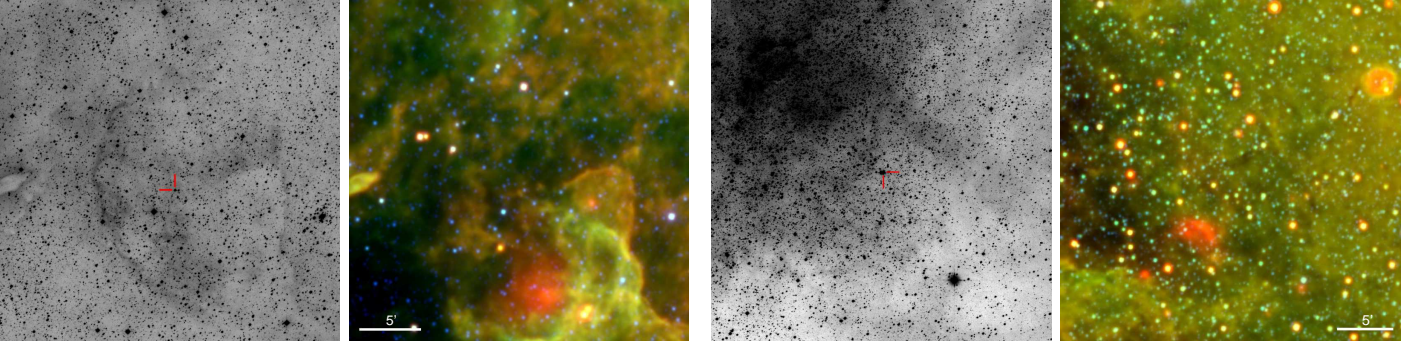


Fig. A.9. Same as Fig. A.1 for WR 68 (G320.5–1.4).

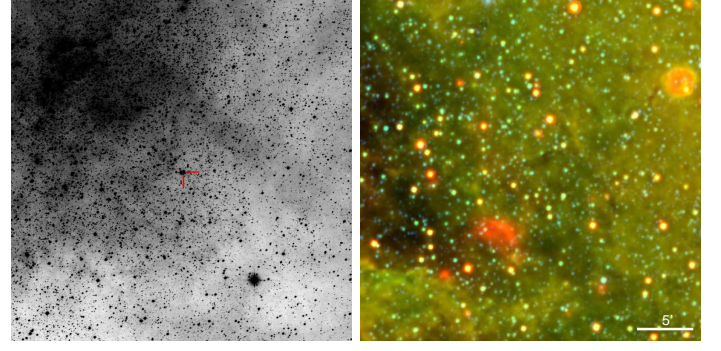


Fig. A.13. Same as Fig. A.1 for WR 94 (Anon)

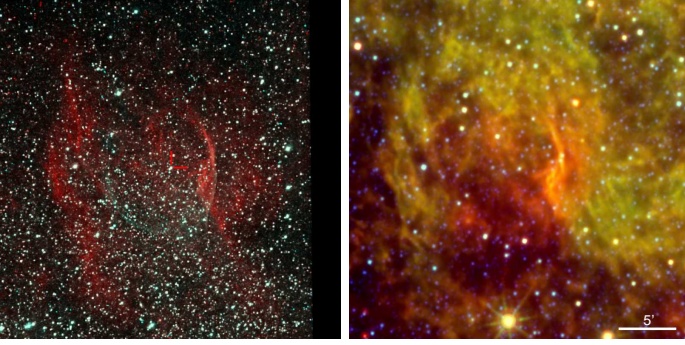


Fig. A.10. Same as Fig. A.1 for WR 75 (RCW 104).

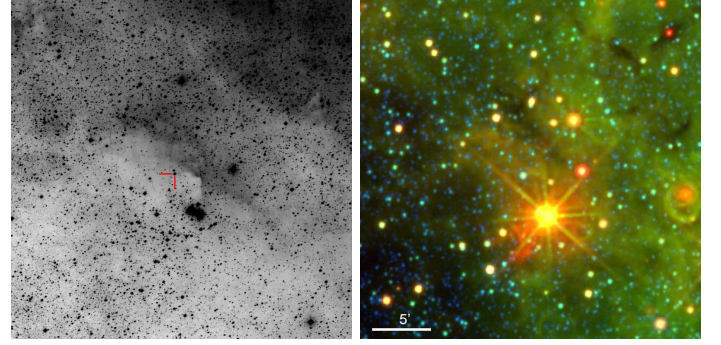


Fig. A.14. Same as Fig. A.1 for WR 95.

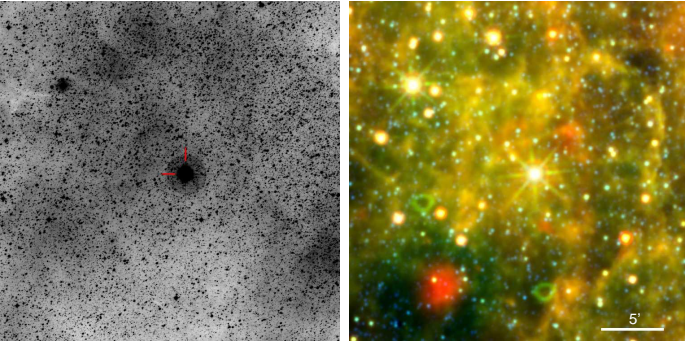


Fig. A.11. Same as Fig. A.1 for WR 85 (RCW 118).

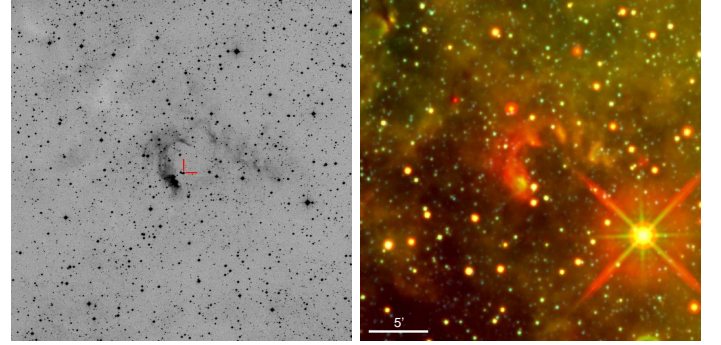


Fig. A.15. Same as Fig. A.1 for WR 101 (Anon).

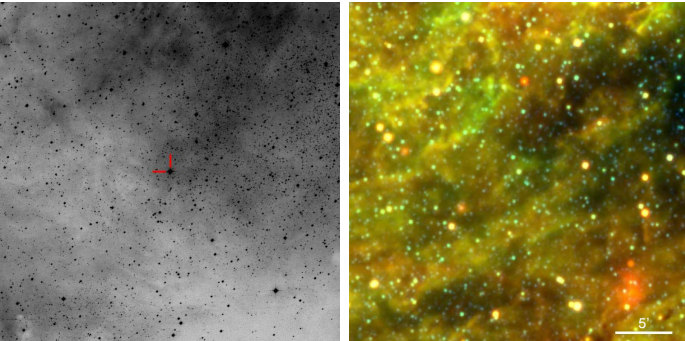


Fig. A.12. Same as Fig. A.1 for WR 86 (RCW 130).

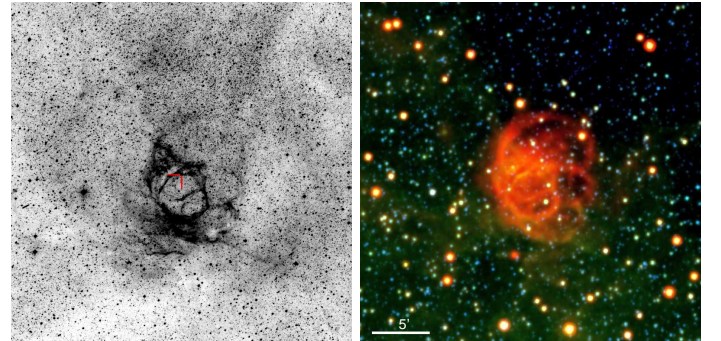


Fig. A.16. Same as Fig. A.1 for WR 102 (G2.4+1.4).

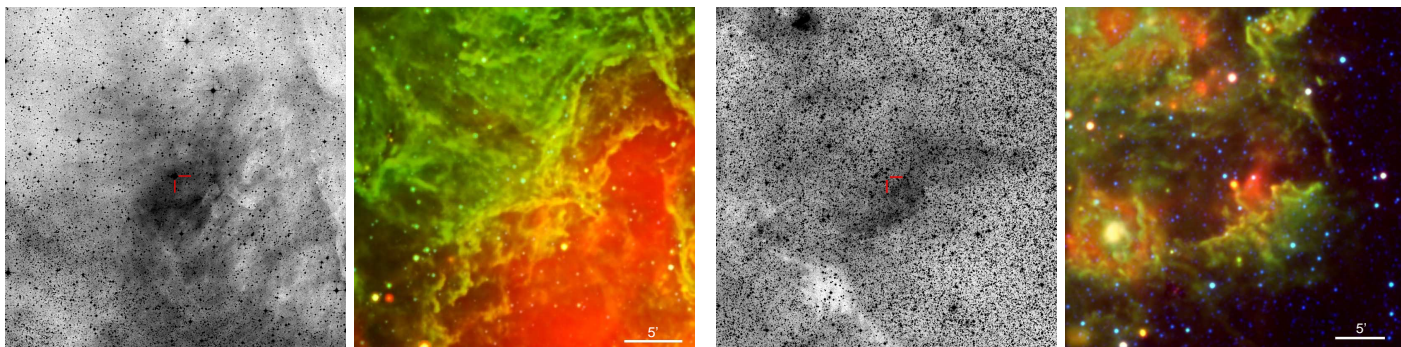


Fig. A.17. Same as Fig. A.1 for WR 113 (RCW 167).

Fig. A.21. Same as Fig. A.1 for WR 131.

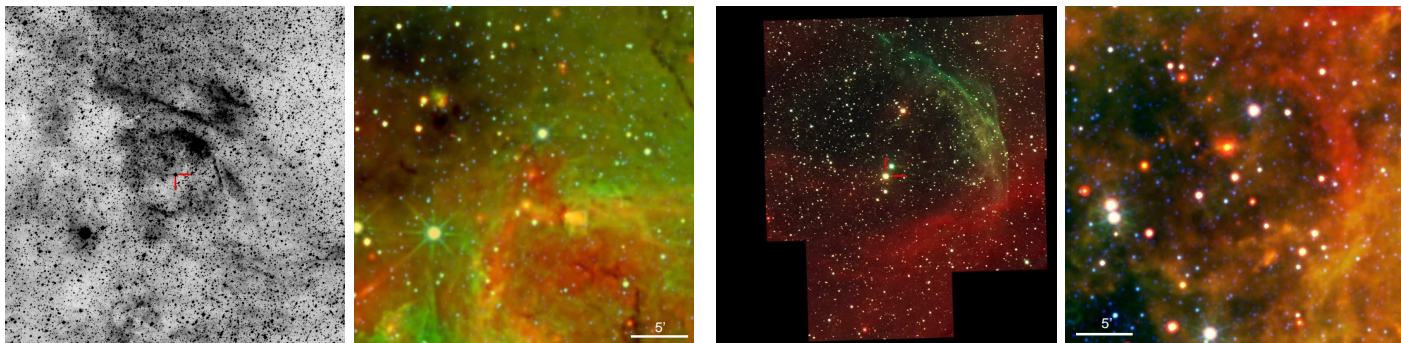


Fig. A.18. Same as Fig. A.1 for WR 116 (Anon).

Fig. A.22. Same as Fig. A.1 for WR 134 (Anon).

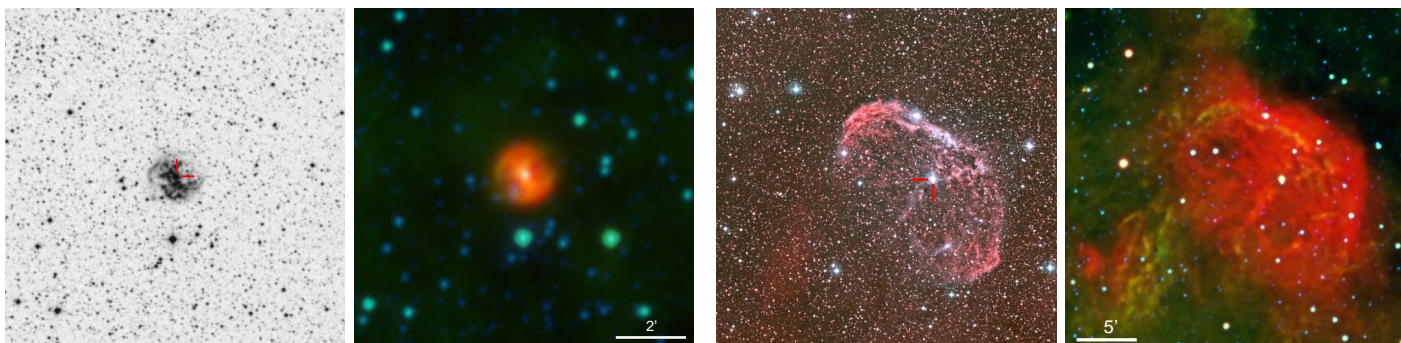


Fig. A.19. Same as Fig. A.1 for WR 124 (M1-67)

Fig. A.23. Same as Fig. A.1 for WR 136 (NGC 6888).



Fig. A.20. Same as Fig. A.1 for WR 128 (Anon).